This manuscript was accepted by J. Chem. Phys. Click here to see the version of record.

A Sequential Nanopore-Channel Device for Polymer Separation

Martin Magill,[1] Ed Waller,[2] and Hendrick W. de Haan[1, a)]

[1)] *Faculty of Science, University of Ontario Institute of Technology, 2000 Simcoe St N, Oshawa, Ontario L1H7K4, Canada*

[2)] *Faculty of Energy Systems and Nuclear Science, University of Ontario Institute of Technology, 2000 Simcoe St N, Oshawa, Ontario L1H7K4, Canada*

(Dated: 13 October 2018)

In this work, we investigated whether a series of nanopores connected by channels can be used to separate polymer mixtures by molecular size. We conducted multiscale coarse-grained simulations of semiflexible polymers driven through such a device. Polymers were modelled as chains of beads near the nanopores and as single particles in the bulk of the channels. Since polymers rarely escape back into the bulk of the channels after coming sufficiently close to the nanopores, the more computationally expensive simulations near the pores were decoupled from those in the bulk. The distribution of polymer positions after many translocations was deduced mathematically from simulations across a single nanopore-channel pair, under the reasonable assumption of identical and independent dynamics in each channel and each nanopore. Our results reveal rich polymer dynamics in the the nanopore-channel device, and suggest that it can indeed produce polymer separation. As expected, the mean time to translocate across a single nanopore increases with chain length. Conversely, the mean time to cross the channels from one nanopore to the next decreases with chain length, as smaller chains explore more of the channel volume between translocations. As such, the time between translocations is a function of the length and width of the channels. Depending on the channel dimensions, polymers are sorted by increasing length, decreasing length, or non-monotonically by length such that polymers of an intermediate size emerge first.

I. INTRODUCTION

Nano- and microfluidic devices show great promise as next-generation polymer separation technologies[1–3]. Potential advantages over traditional separation techniques include faster throughput, higher efficiency, miniaturization and automation (as in lab-on-a-chip designs), and the ability to deal with long polymer chains.

Nanopores, small holes in thin membranes whose diameters and thicknesses are on the order of tens of nanometers, are an important class of nanofluidic devices[2]. They occur pervasively in biological systems, usually formed by membrane-bound proteins, but can also be fabricated synthetically in, for instance, thin films. They have attracted much attention recently for technological applications, especially DNA sequencing[4]. However, since the mean passage time of a polymer forced to translocate through a nanopore is a function of its length, nanopores could also be used for polymer separation. Unfortunately, polymer separation using nanopores has proven challenging in practice, as the translocation process is highly variable[5–7].

In this work, we study a device consisting of a series of nanopores connected by channels. Our hypothesis is that repeated translocation through multiple nanopores in series should exhibit decreased overall variability relative to translocation through a single nanopore, so that this nanopore-channel device could be used for polymer separation. We explore channel dimensions from hundreds to thousands of nanometers, and restrict our attention to cases where polymers can fit in the channels without conformational restrictions. Polymer dynamics in such channels are essentially the same as those in bulk solution[2,3]. Since these channels have no polymer separation power on their own, we consider this device to be a minimalist implementation of multiple nanopores connected in series. Nonetheless, as we will show, the overall separation power of the nanopore-channel device still depends greatly on polymer dynamics in the channels.

In order to study the polymer separation power of these devices, we present a multiscale model of non-interacting semiflexible homopolymers driven by an applied electric field through a series of nanopores connected by cylindrical channels. We analyse simulations of polymers traversing a single channel and a single nanopore to infer the average speed of polymers moving through the entire nanopore-channel device. Our results indicate that polymers can be sorted with good resolution using hundreds to thousands of pores in series. Channel geometry plays a fundamental role in determining the polymer dynamics. For instance, depending on the channel dimensions, the polymers can be sorted into increasing, decreasing, or non-monotonic order by chain length.

We begin by reviewing some of the relevant literature on polymer separation with micro- and nanofluidic devices. Next, we introduce the details of our multiscale model, which models the system at three levels of detail. We then present our simulation results at each of these three scales. We show that the nanopore geometry used here is not especially optimized for polymer separation. This is by design, to demonstrate that the nanopore-channel device provides enhanced polymer separation even without carefully manufactured pores. We also discuss the rich polymer dynamics revealed by simu-

[a)] Electronic mail: Hendrick.deHaan@uoit.ca

lations in the interior of the channels, far from the pores. We derive a simple physical model that accounts for much of the interplay between the polymers' lengths and the channels' dimensions. We finish with results demonstrating the separation of polymers by length as they move through many consecutive nanopores.

A. Background and Related Work

At a high level, the goal of polymer separation can be stated as follows: given a mixture of polymers, group polymers according to some property into distinct spatial regions[8]. For linear polymers, the goal is usually to separate them according to chain length. Unfortunately, some polymers of interest (most notably DNA) are free-draining, which means that chains of different lengths move with the same drift velocity under an applied electric field in bulk solution[3]. As a result, devices for DNA separation must introduce a length-dependence on polymer motion.

Traditional approaches to polymer separation include gel electrophoresis techniques (the physics of which was reviewed, for instance, by Viovy et al.[9]) and capillary electrophoresis methods (which were recently reviewed, for instance, by Harstad et al.[10]). Many nano- and microfluidic devices have been considered for next-generation polymer separation technologies. In a review of this topic, Levy et al. classified these sorting approaches into entropic sorting devices, Brownian ratchets, structured media, and free solution sorting devices[2]. In a separate review, Dorfman et al. explored two classes of sorting devices: post-arrays (which are a subset of what Levy et al. called structured media devices) and slit-well devices (which fall under what Levy et al. called entropic sorting devices)[3].

In entropic sorting devices, length-dependent mobility is created by a series of entropic traps. For instance, this has been accomplished by Han et al. with the slit-well motif, which consists of a series of small nanoslits connected by larger slits, or wells[11,12]. There is an entropic barrier for polymers to enter the small nanoslits from the wells, and the dynamics of this escape process depend on chain length. Specifically, as they can enter the smaller nanoslit by any point along their length, longer chains make the transition more quickly than smaller chains. This device is similar in spirit to the nanopore-channel device considered here, with the nanopores playing the role of the small nanoslits and the channels playing the role of the wells. However, the devices are fundamentally different because the nanoslit device is essentially two-dimensional, whereas nanopores are essentially one-dimensional. For instance, in the nanopore-channel device, chains of all length can only enter the nanopore at a single position, so the primary dynamics of the slit-well motif have no analogue. Another intrinsic difference between the two devices is in the electric field shape. The electric field in the well of the slit-well devices is reduced from that in the slits by a linear ratio of their respective length scales (by conservation of flux). In contrast, the electric field in the channels of the nanopore-channel device is reduced from that in the nanopores by the square of the ratios of the two length scales. Thus the nanopore-channel device intrinsically supports much larger field gradients. Nonetheless, the systems do share some similarities: as we will show, in both systems polymers can exhibit the unusual behaviour of increasing mobility with increasing chain length[3].

As mentioned above, in addition to their use for sequencing applications, nanopores have also previously been considered for polymer separation. Length-dependent motion arises because longer polymers take longer, on average, to translocate through a given nanopore. For instance, Carson et al. and Bell et al. demonstrated experimentally that the length of a translocating DNA chain can be identified by its translocation time[5,6]. Unfortunately, the use of nanopores for polymer separation by length is limited by the intrinsic variability of the translocation process. For instance, typical nanpores cannot identify the length of double-stranded DNA (dsDNA) molecules with better resolution than roughly 1000 bp[6]. By carefully manufacturing nanopores with diameters very close to 3 nm, Carson et al. achieved improved resolutions on the order of 100 bp[5]. Briggs et al. also demonstrated resolution on the order of 100 bp in nanofiltered nanopore devices, where a nanoporous membrane pre-confines DNA molecules before translocation[7]. These innovations improve the sensitivity of the translocation time to chain length by reducing the variability of the translocation process, but this comes at the cost of additional manufacturing requirements.

In principle, a simple way of improving the resolution of any nanopore-based filters would be to use many of them in series. Repeated independent applications of a stochastic filter n times should theoretically reduce the net variability of the process by a factor of $1/\sqrt{n}$. One might therefore hope to simply study a single nanopore in isolation, then extrapolate to determine the filtering potential of n nanopores in series. However, as this work will demonstrate, the precise fashion in which the nanopores are connected is fundamental to the overall polymer dynamics, and cannot be neglected.

To our knowledge, there have not been many previous studies exploring the translocation of polymers through multiple nanopores in series. Langecker et al. conducted experiments with dsDNA in a micron-scale cavity bounded by two nanopores[13]. They used 10 kbp dsDNA and conducted time-of-flight measurements at a variety of voltages. In contrast to the work presented here, those experiments varied voltage but did not vary chain length. Thus those experiments cannot be used directly to speculate about the separation power of nanopores in series. Instead, they demonstrate that nanopores in series can yield more detailed analysis of molecular properties than single nanopores.

II. MODEL AND METHODOLOGY

In this section, we will describe our multiscale model of polymers in the nanopore-channel device, as well as our simulation methodology. The system was modelled at three scales, which will be referred to as the microscopic, mesoscopic, and macroscopic scales in order from finest to coarsest level of detail. Figure 1 summarizes the models used at each scale. At the largest scale (Figure 1(c)), the system geometry consists of nanopores connected in series by channels, with all pores and channels centered on a common axis. The following subsections will describe the model at each scale in turn, and additional details are available in the supplemental materials.

A. Microscopic Model

The microscopic model (Figure 1(a)) was used to capture the dynamics of the molecules near the nanopores. This phase included capture from free solution into the pore and translocation through the pore. This is the most detailed scale in our model, as the polymer dynamics in this region are both complicated and crucial to a proper understanding of the device. The simulations utilized a standard coarse-grained Langevin dynamics (CGLD) polymer consisting of N beads[14]. This level of detail has been used extensively to study polymer translocation through nanopores[15–26]. Simulations were conducted using the ESPResSo software package on the SHARCNET computing facilities[27].

Polymers were constructed using N identical monomers arranged linearly using finitely-extensible nonlinear elastic (FENE) forces to bond monomers and Weeks-Chandler-Anderson (WCA) forces to model excluded volume[14]. The semiflexibility of the chain was modelled using a harmonic potential on the angle formed by any three consecutive monomers along the chain backbone. A persistence length of $L_p = \sigma$ was imposed, where σ is the effective monomer diameter dictated by the WCA interaction. Length scales throughout the remainder of this paper will be expressed in terms of this effective chain width σ. This choice was motivated by double-stranded DNA molecules, which have an effective width of a few nanometers (larger than the steric width ≈ 2.5 nm) and a persistence length of roughly $30 - 50$ nm[28–31]. As discussed in the supplemental material, the aspect ratio of the model polymer was somewhat smaller than that of real DNA, which enabled longer polymers to be simulated.

WCA forces were also used to apply purely repulsive interactions between monomers and the nanopore walls. An effective nanopore radius of 0.8 was used. This radius was selected as it only enabled polymers to traverse the pore by an end, i.e. polymers could not enter the pore in a folded configuration. This simplified the current analysis, but future work will explore the impact of folding dynamics.

The thermal motion of the polymer was modelled via Langevin dynamics. The thermostat used a thermal energy of $kT = 1$ and a friction coefficient of $\gamma = 1$ for each monomer, and the monomer mass was $m = 1$ as well. Translocation was driven by an electric force field. The shape of the electric field in the microscopic region was approximated by the analytic solution for the electric field of a nanopore in an infinite unbounded domain[32]. This is a good approximation when the channel dimensions are much larger than the pore radius, which is the case for all simulations in this paper. The advantage of this approximation is that the results of the microscopic simulations become independent of the channel geometry, enormously improving the computational efficiency of the model. The magnitude of the electric field was scaled to match the Péclet number of the simulations to relevant experimental conditions for dsDNA translocation, as discussed in the supplemental material[33].

At the start of the microscopic simulations, polymers were initialized in an equilibrated conformation a distance $r_{\text{cap}} = N/4$ from the nanopore. This distance was chosen to balance two effects. We found that this r_{cap} was far enough from the pore that the electric field strength was not strong enough to significantly deform the polymer conformations from equilibrium as they diffused around that distance. Conversely, this r_{cap} was also close enough to the pore that the electric field was strong enough that polymers were unlikely to diffuse very far from the pore before translocating. See the supplemental material for more details.

The primary measurement in the microscopic model was the microscopic time, defined as the time after the release of a polymer (i.e. after equilibration) until all of its monomers were located on the *trans* side of the nanopore. If polymers ever moved far enough away from the pore that the closest monomer to the pore was farther than the cut-off radius of N from the pore, then the event was considered a failure. Failed events were restarted, so that the total number of successful translocations measured at each chain length was 2000.

B. Mesoscopic Model

The mesoscopic model (Figure 1(b)) was used to study the dynamics farther from the nanopores, in the bulk of the channels. In this region, the electric field gradient was small over the length scale of the polymer, so that it could not significantly deform the polymer conformations. In other words, these dynamics were dominated by the translational motion of the center of mass. As such, in the mesoscopic model each polymer was represented by a single effective particle, and was simulated using coarse-grained Brownian dynamics (CGBD)[14].

The mesoscopic CGBD simulations were made compatible with the microscopic CGLD simulation conditions. The diffusion coefficients of the mesoscopic particles were set to $1/N$, corresponding to the center of

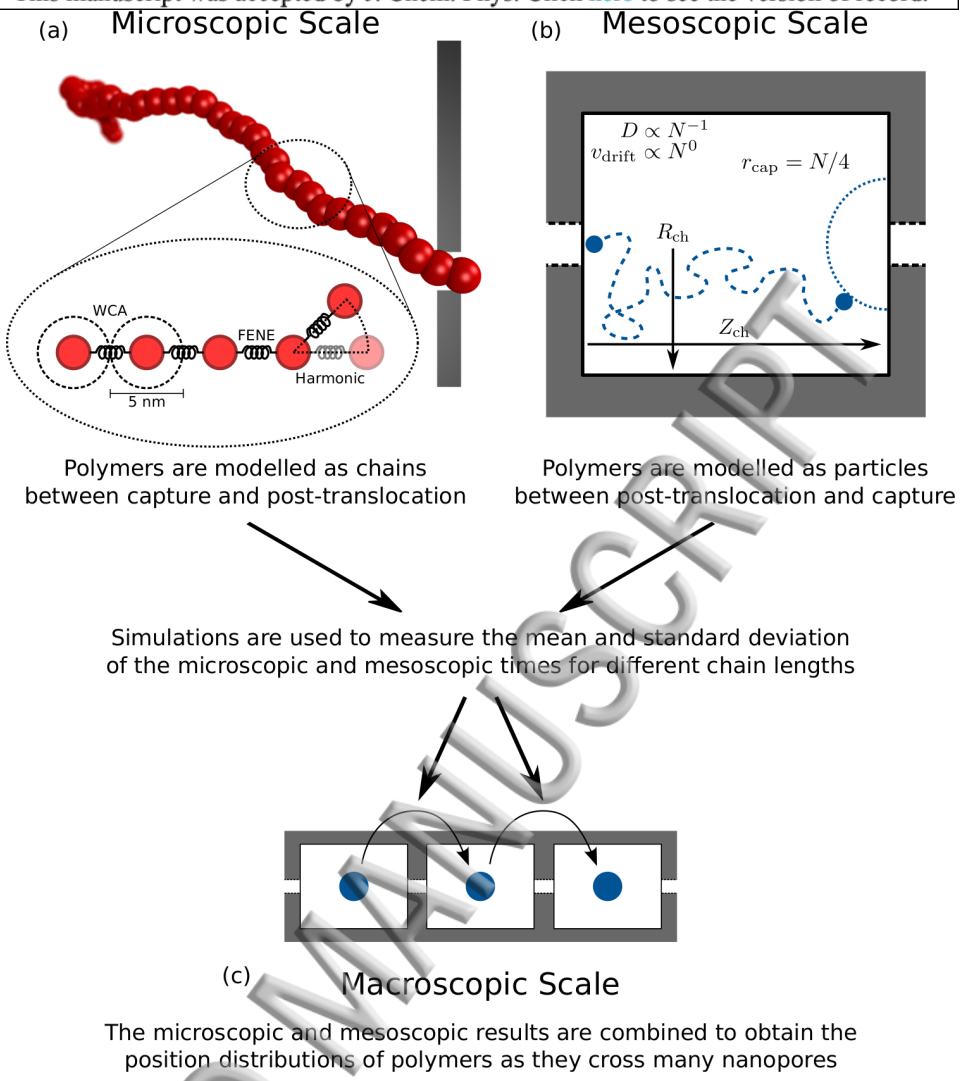

FIG. 1. Schematics illustrating the three modelling scales used for this system. (a) In the microscopic model, WCA and FENE interactions were used to construct a linear homopolymer of N beads, and harmonic angular potentials were used to implement semiflexibility. (b) At the mesoscopic scale, the entire polymer was represented by a single Brownian particle. Simulations were initialized with particles at the inlet pore of a channel of radius R_{ch} and length Z_{ch}, and terminated when particles were absorbed near the outgoing pore. (c) At the macroscopic scale, the net motion of polymers through the nanopore-channel device was inferred by treating each of the consecutive nanopore-channel pairs as identical and independent subunits of the device.

mass diffusion coefficients predicted by the Rouse model for polymers of length N in the microscopic model. The CGBD thermostat and force magnitudes were set as in the microscopic model, with each polymer experiencing a net friction coefficient equal to N times the monomer γ, in accordance with the Rouse model. Similarly, each CGBD chain experienced a net force equal to N times the force that a single monomer would feel. As a result, large chains diffused more slowly than smaller chains, but all chains exhibited identical free solution electrophoretic drift velocities.

The electric field in the mesoscopic model was obtained by solving Laplace's equation in cylindrical coordinates using the finite element method with the FEniCS software package[34]. The channel was modelled as a cylinder of length Z_{ch} and radius R_{ch} (see Figure 1(b)). The mesoscopic simulations were initialized with particles in the inlet nanopore of a channel, and proceeded until the particles contacted the hemisphere of radius $r_{\text{cap}} = N/4$ surrounding the outgoing nanopore. We call the first passage time for particles to reach this absorbing hemispherical boundary the mesoscopic time.

As stated above, the starting radius of the microscopic model is included in the mesoscopic model as an absorbing boundary. As argued in the supplemental material, this is valid because it was possible to choose a set of capture radii $r_{\text{cap}} = N/4$ such that the failure rate was simultaneously small for all chain lengths. However, the

failure rate is counted by the number of events that diffuse to a distance of $4r_{\mathrm{cap}}$ from the pore. Within that distance, the microscopic model neglects the channel walls, which is a limitation of the current model. Nevertheless, the computational benefit of neglecting the channel walls in the microscopic model is enormous, as it enables the same microscopic results to be used across many channel geometries. To justify the use of this simplifying assumption, the mesoscopic model was only studied for polymer chains that satisfied the condition that

$$\min(R_{\mathrm{ch}}, Z_{\mathrm{ch}}) > r_{\mathrm{cap}} + R_G, \tag{1}$$

where R_G is the radius of gyration and was approximated with the wormlike chain model,

$$R_G \approx \left[\frac{L_p N}{3} - L_p^2 + \frac{2L_p^3}{N}\left(1 - \frac{L_p}{N}\left(1 - e^{-\frac{N}{L_p}}\right)\right)\right]^{1/2}, \tag{2}$$

where N is the nominal contour length and $L_p = 10$ is the persistence length[35]. This restriction reduces the influence of omitting the walls from the microscopic model, since it ensures that the walls are far from the pore, where the electric field is weak. Furthermore, it also ensures that the polymers have R_G much smaller than the dimensions of the channel, which is another assumption of the model.

C. Macroscopic Model

The transport of polymers across multiple channels was captured in the macroscopic model. The behaviour of polymers at this scale was solved analytically on the assumption that their dynamics in distinct nanopores and channels were independent and identical. When this is the case, the macroscopic dynamics are entirely determined by the micro- and mesoscopic dynamics in any given channel.

Since the boundary between the microscopic and mesoscopic domains was chosen such that the rate of transport from the microscopic zone back into the mesoscopic region was negligible, the time to cross a given nanochannel, t_{macro}, can be approximately modelled as

$$t_{\mathrm{macro}} = t_{\mathrm{micro}} + t_{\mathrm{meso}}, \tag{3}$$

where t_{micro} and t_{meso}, the times to cross the respective subdomains, are statistically independent. Thus the probability density function of t_{macro} is the convolution of the other two variables', i.e.

$$\rho(t_{\mathrm{macro}}) = \rho(t_{\mathrm{micro}}) * \rho(t_{\mathrm{meso}}). \tag{4}$$

Similarly, the probability density function of the time at which the polymer will enter the kth channel for the first time, $t(k)$, is given by

$$\rho(t(k)) = \underbrace{\rho(t_{\mathrm{macro}}) * \rho(t_{\mathrm{macro}}) * \ldots * \rho(t_{\mathrm{macro}})}_{k \text{ times}}. \tag{5}$$

Equation 5 for the distribution of $t(k)$ can be computed directly from the distributions of t_{micro} and t_{meso}. However, by the central limit theorem, $\rho(t(k))$ will converge in the limit of large k to

$$\rho(t(k)) \approx \mathcal{N}(k\mu_{\mathrm{macro}}, k\sigma^2_{\mathrm{macro}}), \tag{6}$$

where μ_{macro} and $\sigma^2_{\mathrm{macro}}$ are the mean and variance, respectively, of t_{macro}, and $\mathcal{N}(\mu, \sigma^2)$ denotes a normal distribution. This approach treats k as a continuous random variable when it is in fact discrete; this is justified for large values of k.

From this, we derive the distribution of polymer positions as a function of channel number k. The probability of a polymer being in channel $k' \geq k$ at time t is given by

$$p(k' \geq k) = p(t(k_0) \leq t) = \int_0^t p(t(k) = t')dt' \tag{7}$$

$$\approx \frac{1}{2}\left(1 + \mathrm{erf}\left(\frac{t - k\mu_{\mathrm{macro}}}{\sqrt{2k\sigma^2_{\mathrm{macro}}}}\right)\right) \tag{8}$$

when k is large enough to apply the central limit theorem to $\rho(t(k))$. This is the cumulative distribution of polymer position in the macroscopic system. To obtain the corresponding probability density function, we take the derivative, and see that the position distribution over k at time t is

$$\rho(k;t) \approx \frac{-\partial p(k' \geq k)}{\partial k} \tag{9}$$

$$= \frac{t + k\mu_{\mathrm{macro}}}{\sqrt{8\pi k^3 \sigma^2_{\mathrm{macro}}}} \exp\left(-\frac{(t - k\mu_{\mathrm{macro}})^2}{2k\sigma^2_{\mathrm{macro}}}\right). \tag{10}$$

Finally, we can apply the central limit theorem again to find that the position distribution when t is large is given by

$$\lim_{t\to\infty} \rho(k;t) = \mathcal{N}\left(\frac{\sigma^2 + 2\mu t}{2\mu^2}, \frac{5\sigma^4}{4\mu^4} + \frac{\sigma^2 t}{\mu^3}\right) \tag{11}$$

$$= \mathcal{N}\left(\frac{t}{\mu} + \frac{1}{2}\left(\frac{\sigma}{\mu}\right)^2, \left(\frac{\sigma}{\mu}\right)^2 \frac{t}{\mu} + \frac{5}{4}\left(\frac{\sigma}{\mu}\right)^4\right), \tag{12}$$

where μ and σ are the mean and variance of t_{macro}, but the subscripts have been omitted for ease of reading. The mean and variance of $\rho(k;t)$ were calculated using Mathematica 11.1[36].

Equation 12 can be used to compute the position distribution's coefficient of variation CV, which is its standard deviation divided by its mean. This describes the relative width of the distribution. In the limit of large t, the coefficient of variation will approach

$$\lim_{t\to\infty} CV = \frac{\sigma}{\sqrt{\mu}}\frac{1}{\sqrt{t}} \propto \frac{1}{\sqrt{t}}. \tag{13}$$

Thus, although the position distributions become arbitrarily broad at large times, they become progressively narrower relative to the mean displacement.

Furthermore, when t is large, the mean polymer position given by Equation 12 will be roughly t/μ_{macro}, and so the mean polymer speeds through the nanopore-channel device will approach $1/\mu_{\text{macro}}$. Since $\mu_{\text{macro}} = \mu_{\text{micro}} + \mu_{\text{meso}}$ by linearity, the mean position of polymers after many translocations depends equally on the microscopic and mesoscopic dynamics. The same conclusion applies to the variance of the position distribution. In other words, one cannot consider the filtering effect of a series of nanopores without also considering the exact process by which polymers are fed from one nanopore into the next. As will be shown below, the mesoscopic dynamics are quite rich, and can in fact be more important than the microscopic dynamics.

III. SIMULATION RESULTS

In this section, we present the results of our simulations at the microscopic, mesoscopic, and macroscopic scales, in that order.

A. Results at the Microscopic Scale

The microscopic simulations were conducted for chains of length $N = 10, 20, 50, 75, 100, 150,$ and 200. Figures 2(a) and 2(b) show the mean and variance, respectively, of the microscopic time. Recall that the microscopic time includes *both* the translocation time, which is commonly studied, as well as the capture time, which is the time for the polymer to enter the nanopore after the start of simulation. The capture process has often been neglected in the literature, although recent work has shown that it can radically alter the subsequent translocation process[26].

Figures 2(a) and 2(b) demonstrate that the mean and variance of the microscopic time increase monotonically with chain length over the range studied here. Although our results do not suggest that the mean and variance of microscopic time are related to the chain length N by power laws, it is still interesting to consider the approximate scaling of these quantities with N. Linear regression between the logarithms of the respective quantities yields:

$$\mu_{\text{micro}} \approx 0.98 N^{2.09} \tag{14}$$

$$\sigma^2_{\text{micro}} \approx 2.87 N^{4.01}. \tag{15}$$

Simulation studies measuring the scaling of just the mean translocation time with N under conditions similar to those used here have generally reported exponents in the range of 1.2 to 1.6[16–26]. Conversely, the mean microscopic time measured here increases scales with N to an exponent of roughly 2.09. The fact that the microscopic time contains the capture time in addition to the translocation time is likely a major factor in this discrepancy. In fact, the capture radius $r_{\text{cap}} = N/4$ was increased in proportion to chain length, further complicating a direct comparison between microscopic time and translocation time. Actually, given these significant differences between the two quantities, it is remarkable that their scaling with N is so similar.

It is also interesting to consider the intrinsic polymer separation power of the nanopores studied here. Figure 2(c) contains violin plots of the microscopic times, from which microscopic time distributions can be compared directly between different values of N. It is clear from Figure 2(c) that the microscopic time distributions are heavy-tailed at every chain length, and that there is a significant amount of overlap between distributions for different chain lengths. Thus the current nanopore setup does not appear to be optimized for separation applications. We chose such a nanopore because the goal of the present work is to demonstrate that even nanopores that clearly could not be used to separate polymers in a single pass can successfully separate polymers when connected in series. Of course, nanopore-channel devices constructed using nanopores with superior length resolution, like those demonstrated by Carson et al. or Briggs et al., would be expected to achieve even better polymer separation[5,7].

B. Results at the Mesoscopic Scale

Figure 3(a) shows the mean mesoscopic time for the same range of chain lengths N as used in the microscopic model, as well as for $N = 300$, all for various combinations of the channel dimensions $(R_{\text{ch}}, Z_{\text{ch}})$. Also shown is the mean microscopic time, for comparison. Mesoscopic simulations were run for every combination of R_{ch} and Z_{ch} both in $\{30, 45, 60, 75, 90, 150, 300\}$; and for every combination of Z_{ch} in $\{500, 1000\}$ and R_{ch} in $\{50, 100, 500\}$. The channel lengths, Z_{ch}, are shown by line color; different lines of the same color correspond to different channel radii, R_{ch}, such that the mean t_{meso} increases monotonically with R_{ch} in all cases. Only choices of $(N, R_{\text{ch}}, Z_{\text{ch}})$ that satisfy the restriction of Equation 1 were studied.

Some dependence of the mean t_{meso} on chain length is apparent: in all cases, longer chains cross the mesoscopic region somewhat faster than shorter chains. However, the extent of this effect depends greatly on the channel dimensions. In particular, mesoscopic time is only comparable to microscopic time when the channel volume is small. In large channels, mesoscopic time is much larger than microscopic time; furthermore, it changes very little with chain length. This suggests that connecting nanopores in series with large gaps of bulk solution between them will not lead to any polymer separation, because the thermal motion between subsequent pores will overwhelm the length sensitivity introduced by the

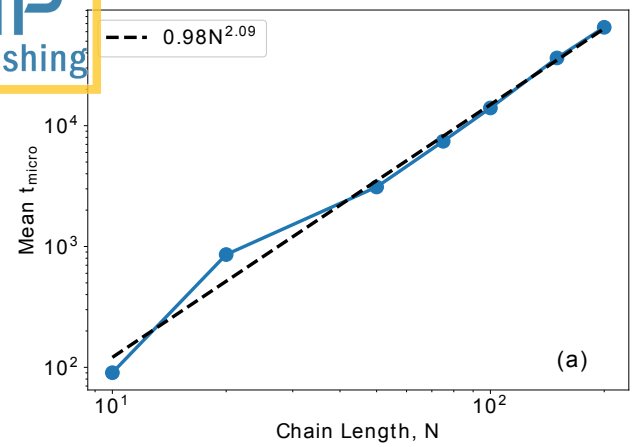

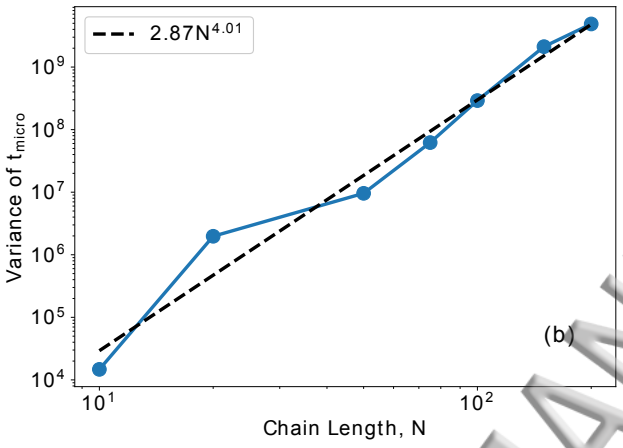

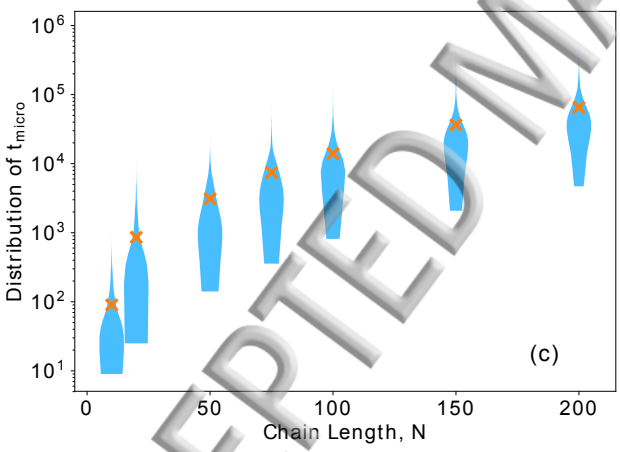

FIG. 2. Results of the microscopic simulations. (a) The mean of the microscopic time, t_{micro}, as a function of chain length. Error bars of one standard error are much smaller than the marker size. (b) The variance of t_{micro} as a function of chain length. (c) Violin plots showing distributions of t_{micro} as a function of chain length. The markers indicate the mean of each distribution.

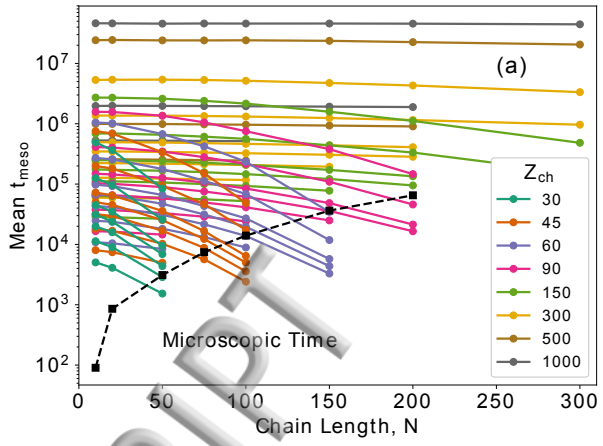

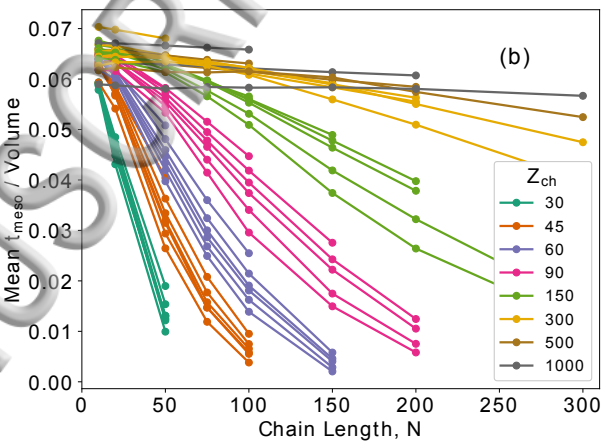

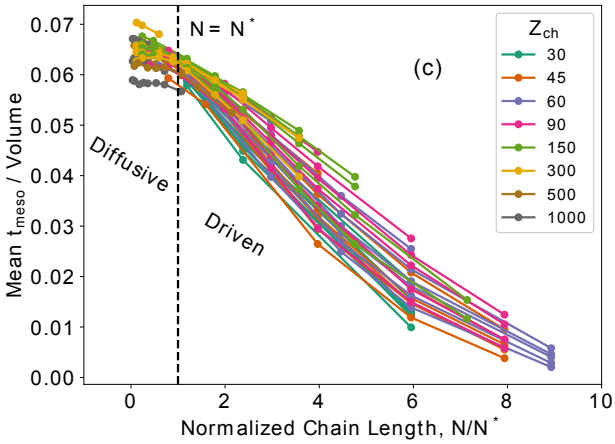

FIG. 3. In all three plots, line color indicates channel length Z_{ch}. Different lines of the same color correspond to different channel radii R_{ch} such that the mean of the mesoscopic time, t_{meso}, always increases monotonically with R_{ch}. (a) Mean t_{meso} for a range of chain lengths in channels of various dimensions $(R_{\mathrm{ch}}, Z_{\mathrm{ch}})$. The dashed line shows the microscopic time. (b) Mean t_{meso} normalized by mesoscopic volume for a range of chain lengths in channels of various dimensions. (c) Mean t_{meso} normalized by mesoscopic volume shown as a function of the normalized chain length N/N^* (discussed in the text) in channels of various dimensions.

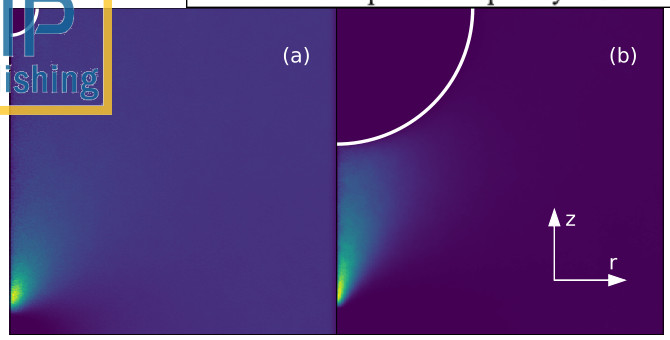

FIG. 4. Heatmaps of g_0 (see text) comparing two mesoscopic simulations in the same nanochannel geometry of $(R_{\mathrm{ch}}, Z_{\mathrm{ch}}) = (30, 30)$ (a) for $N = 10$, and (b) for $N = 50$. Brightness indicates the average residence time of polymers in each region of the channel before reaching the absorbing boundaries (shown in white). Longer chains spend less time far from the axis of the channel.

pores.

Some of the mesoscopic dynamics can be understood by considering particle trajectories. Figure 4 illustrates two typical mesoscopic simulations. The heatmaps show numerical measurements of the time-integrated position probability density throughout the channel (in cylindrical coordinates). These distributions, which will be referred to as g_0, show the average residence time of polymers in each region of the channel before absorption near the exit nanopore. The integral of g_0 over the channel volume equals the mean mesoscopic time[37]. Figure 4 highlights the most important influence of chain length N on dynamics in the mesoscopic simulations. The plot for $N = 10$ shows a g_0 distribution that is nearly uniform over the entire channel, illustrating that these short chains typically diffuse throughout the entire channel before being captured. Conversely, the longer chains with $N = 50$ typically drift axially into the capture radius without diffusing very far in the radial direction. As a result, the average residence time g_0 decays rapidly towards zero away from the channel axis.

Nearly-uniform g_0 distributions, like the one in Figure 4(a), are typical when the channel volume is large or the polymer chain length is small. We will refer to such conditions as the diffusive regime. Since t_{meso} is the volume integral of g_0, it follows that normalizing Figure 3(a) by channel volume might account for some of the dependence of t_{meso} on channel geometry. Figure 3(b) shows this by plotting the following:

$$\frac{t_{\mathrm{meso}}}{V_{\mathrm{meso}}} = \frac{t_{\mathrm{meso}}}{\pi R_{\mathrm{ch}}^2 Z_{\mathrm{ch}} - \frac{1}{2}\frac{4}{3}\pi r_{cap}^3}. \tag{16}$$

As expected, $t_{\mathrm{meso}}/V_{\mathrm{meso}}$ is nearly independent of N, R_{ch}, and Z_{ch} in the diffusive regime.

The remaining mesoscopic dynamics arise for chains that are long enough to drift axially into the capture radius without first diffusing throughout the channel volume (as in Figure 4(b)). We will call such conditions the driven regime. We can estimate the chain length at which the dynamics transition between the diffusive and driven regimes by comparing the characteristic timescales of axial drift and radial diffusion.

The characteristic timescale on which particles drift axially across the channel is

$$\tau_{\mathrm{drift},z} \sim \frac{Z_{\mathrm{ch}} - r_{\mathrm{cap}}}{v_{\mathrm{drift},z}}, \tag{17}$$

where $v_{\mathrm{drift},z}$, the characteristic axial drift velocity, is roughly

$$v_{\mathrm{drift},z} \sim (NF_z^c)(\gamma/N) = F_z^c\gamma, \tag{18}$$

where F_z^c is the characteristic axial force in the bulk of the channel. The characteristic force in the bulk of the channel can be expressed as

$$F_z^c \approx F_p^* \left(\frac{r_p}{R_{\mathrm{ch}}}\right)^2, \tag{19}$$

where $F_p^* \approx 5.19$ is the average axial force in the pore (after tuning the Péclet number; see the supplemental material), and r_p is the radius of the pore. Altogether, then, the characteristic timescale for drifting across the channel is

$$\tau_{\mathrm{drift},z} \sim \frac{Z_{\mathrm{ch}} - \frac{N}{4}}{\gamma F_p^*}\left(\frac{R_{\mathrm{ch}}}{r_p}\right)^2, \tag{20}$$

using $r_{\mathrm{cap}} = N/4$.

The characteristic timescale on which particles diffuse radially is

$$\tau_{\mathrm{diff},r} \sim \frac{R_{\mathrm{ch}}^2}{D} = \frac{R_{\mathrm{ch}}^2}{\frac{k_BT}{\gamma N}} = \frac{N\gamma R_{\mathrm{ch}}^2}{k_BT}, \tag{21}$$

Setting this equal to the characteristic drift time yields

$$N^* = Z_{\mathrm{ch}} \Big/ \left(\frac{1}{4} + \frac{\gamma^2 F_p^* r_p^2}{k_BT}\right) \approx \frac{Z_{\mathrm{ch}}}{3.57}. \tag{22}$$

It is interesting to note that this estimate of N^* does not depend on R_{ch}. This fortuitous result arises because the magnitude of the axial electric field in the bulk of the channel decreases with R_{ch} with the same scaling as the radial diffusion time.

In the same way that normalizing time by V_{meso} accounted for most of the mesoscopic dynamics in the diffusive regime, the dynamics in the driven regime can be accounted for by normalizing the chain lengths by N^*. As shown in Figure 3(c), plotting $t_{\mathrm{meso}}/V_{\mathrm{meso}}$ against N/N^* produces nearly the same curve for all channel geometries currently under consideration. In other words, the mean mesoscopic time is, to a reasonably good approximation, a function of the channel volume and N^*.

Overall, Figure 3 clearly demonstrates that t_{meso} generally decreases monotonically with N. This is in direct

contrast to t_{micro}, which increases monotonically with N. In the next section, we will show that the interplay between these trends can be exploited to sort polymers into increasing, decreasing, or non-monotonic functions of N, depending on the relative magnitudes of t_{micro} and t_{meso}.

The standard deviation of the mesoscopic time, σ_{meso}, also plays an important role in ultimately understanding the macroscopic dynamics of the device. Unfortunately, it was not possible to find a simple characterization of σ_{meso} comparable to that obtained above for μ_{meso}. To some extent, larger channels produce larger standard deviations. The details are more complicated than this, and are shown in the supplemental information. Detailed characterization is left to future work, as the purpose of the present work is primarily to show that the nanopore-channel device can indeed sort polymers under reasonable experimental conditions.

C. Results at the Macroscopic Scale

Finally, we will combine the results of the previous two sections to compute the dynamics of polymers at the macroscopic scale, after they have crossed many consecutive pores in the nanopore-channel device. In particular, this section will show results with three choices of the channel dimensions, which cause polymers to become sorted into increasing, decreasing, and non-monotonic orders by length, respectively. Furthermore, we will discuss some of the general qualitative trends that are suggested by our analysis.

1. Sorting into Monotonically Increasing Order of Length

Recall that the microscopic time always increases with chain length N, whereas the mesoscopic time always decreases with N. To produce sorting in increasing order of length, then, the geometry must be chosen so that $t_{\text{micro}} \gg t_{\text{meso}}$. As summarized in Figure 3, the mean t_{meso} can be made smaller at all chain lengths by reducing channel volume. Conversely, decreasing the channel length Z_{ch} accentuates the decrease of the mean t_{meso} with N, which is counterproductive in the pursuit of increasing sorting. Thus to produce increasing sorting one must choose a channel with a small volume but a large Z_{ch}; therefore, R_{ch} must be small.

Figures 5(a) and (d) show results at the macroscopic scale for a device with $(R_{\text{ch}}, Z_{\text{ch}}) = (30, 90)$. Figure 5(a) shows the time evolution of the approximated means and standard deviations of the polymer position distributions over the channel number k. Specifically, these are obtained by combining the results of the microscopic and mesoscopic simulations at each value of N with Equation 12, which is valid for large k. The inset of Figure 5(a) shows $1/\mu_{\text{macro}}$ as a function of N, which we previously argued is the average polymer speed in the long-time limit. Conversely, Figure 5(d) shows the detailed position distributions for each chain length, computed using Equation 10, after 40 million units of simulation time. These results demonstrate increasing sorting by chain length N over this range of chain lengths.

Figure 5(a) shows that good separation occurs after a very large number of channels. In practice, it is likely desirable from a manufacturing point of view to minimize the number of requisite channels. For increasing sorting, this can be accomplished by increasing the magnitude of t_{micro}. Future work will explore options for accomplishing this, such as by using a nanopore with an internal cavity. As shown in previous work, when the cavity size is slightly smaller than R_G, it acts as an entropic trap, greatly increasing the translocation time[38].

2. Sorting into Monotonically Decreasing Order of Length

Next, we will demonstrate decreasing sorting by length. In this case, in contrast to the previous section, the geometry must be chosen so that $t_{\text{micro}} \ll t_{\text{meso}}$. This is accomplished by making the channel volume large. However, as Z_{ch} increases, the dependence of t_{meso} on N becomes less pronounced, which reduces the separation power of the device. Thus decreasing sorting occurs when the volume is large and Z_{ch} is small, in direct contrast to increasing sorting.

Figures 5(c) and (f) demonstrate decreasing sorting in a channel with $(R_{\text{ch}}, Z_{\text{ch}}) = (90, 45)$. Good separation is achieved with far fewer channels than for increasing sorting. This can be understood as follows. Sorting into decreasing order of length relies on the dependence of t_{meso} on N. As shown in Figure 3(c), increasing R_{ch} increases the mean mesoscopic time without significantly changing the dependence of t_{meso} on N. As a result, the difference in t_{meso} between short and long chains can be made large by increasing R_{ch}, increasing the sorting power per channel.

On the other hand, increasing R_{ch} too much compromises the filtering effect, as it broadens the position distributions. This broadening arises because in very wide, short channels, most of the channel volume is far from the axis, where the electric field is weak. Polymers that diffuse away from the axis before crossing the length of the channel axially remain trapped in the channel for a long time. Conversely, since the channel is also short, polymers will occasionally drift axially straight from pore to pore without first diffusing far from the channel axis. As a result, the spread in mesoscopic times is very large, which leads to a broadening of the macroscopic position distributions.

3. Sorting into Non-Monotonic Order of Length

The strictly increasing or decreasing sorting cases are extreme presentations of the nanopore-nanochannel device. In general, the device will sort polymers into a non-

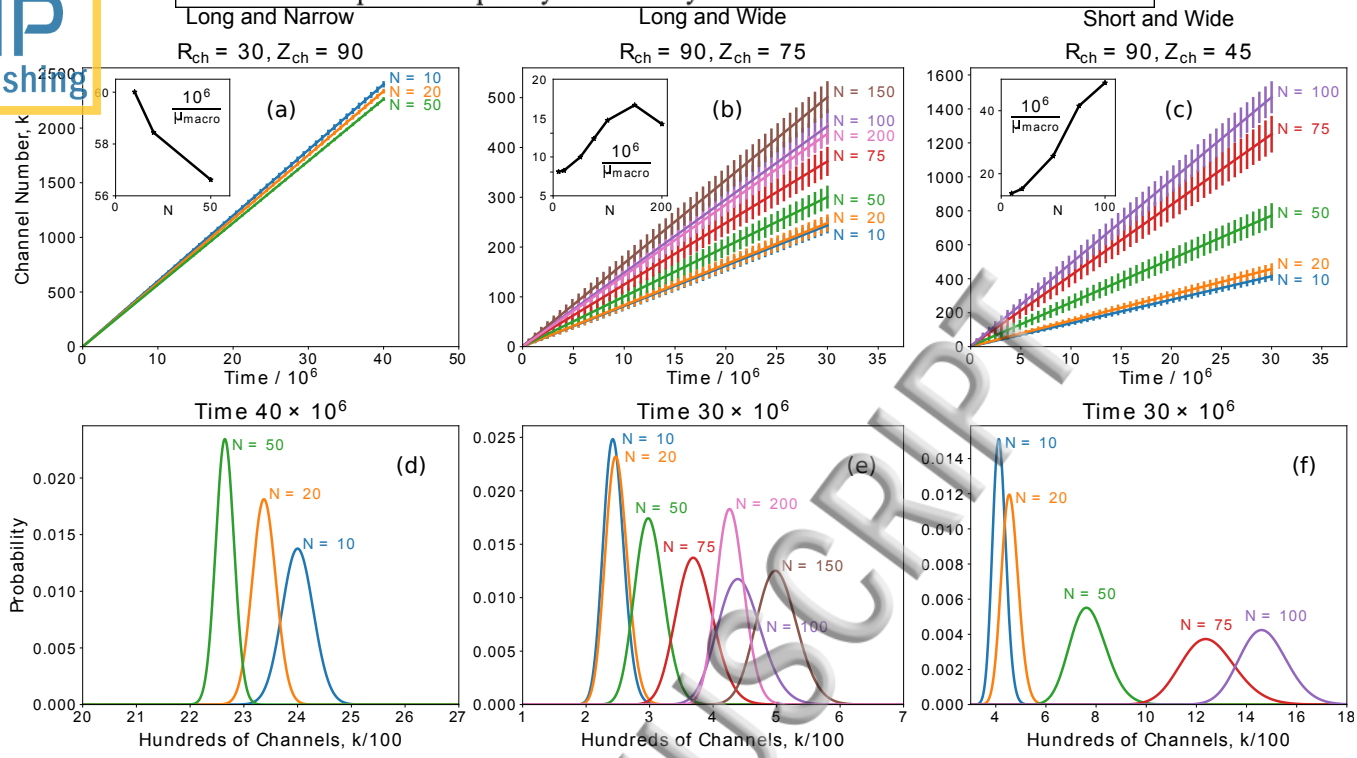

FIG. 5. Results of the simulations at the macroscopic scale. Lines are labeled and colored by chain length N. (a), (b), and (c) show means and standard deviations of polymer positions over channel number k as a function of time, whereas (d), (e), (f) shows the complete polymer position distributions over k at fixed moments in time. The insets in (a), (b), and (c) show the (rescaled) average polymer speeds at large time, $10^6/\mu_{\mathrm{macro}}$, against chain length N. Note that μ_{macro} denotes the mean macroscopic time. (a) and (d) demonstrate sorting into an increasing order of chain length in a long and narrow geometry, with $(R_{\mathrm{ch}}, Z_{\mathrm{ch}}) = (30, 90)$; (b) and (e) demonstrate sorting into a non-monotonic order of length in a long and wide geometry, with $(R_{\mathrm{ch}}, Z_{\mathrm{ch}}) = (90, 75)$; and (c) and (f) demonstrate sorting into a decreasing order of chain length in a short and wide geometry, with $(R_{\mathrm{ch}}, Z_{\mathrm{ch}}) = (90, 45)$.

monotonic order by length because typically $t_{\mathrm{micro}} \ll t_{\mathrm{meso}}$ for short chains, whereas $t_{\mathrm{meso}} \ll t_{\mathrm{micro}}$ for sufficiently long chains. Following the reasoning of the previous two sections, then, short chains will be sorted into decreasing order of length, and long chains will be sorted into increasing order of length. Specifically, chains of some intermediate length will traverse the nanopore-channel device more quickly than both shorter and longer chains.

Figures 5(b) and (e) demonstrate this non-monotonic sorting in a channel with $(R_{\mathrm{ch}}, Z_{\mathrm{ch}}) = (90, 75)$. In this configuration, the chains with $N = 150$ move faster than all the other chains lengths. This type of behaviour is ideal for applications where a specific population of chains must be isolated from both longer and shorter chains. Conversely, the population of chains with $N = 200$ was not separated from the chains with $N \approx 100$. This is inevitable in a situation where speed is a non-monotonic function of N. Nonetheless, this example demonstrates that good separation can still be achieved among the chains that are smaller than the fastest chain length (e.g. $N = 50$ from $N = 75$, in this case), and also among chains that are longer than the fastest chain length (e.g. $N = 150$ from $N = 200$, in this case). In fact, among these two populations, good separation is achieved in this example using fewer channels than required in either of the previous two examples. In this sense, the device producing non-monotonic sorting demonstrated better separation power per nanopore than those producing monotonic sorting.

IV. CONCLUSIONS

We have demonstrated that polymers can be sorted by length using a series of nanopores connected by channels. Good length separation was observed despite the relatively poor length sensitivity of the specific nanopore geometry studied here.

Our results clearly indicate that the polymer dynamics in the channels cannot be neglected, even though the channels have no intrinsic separation power in the absence of the nanopores. In fact, whereas ignoring the channels (for instance, by assuming t_{macro} consists of only translocation time) would lead one to expect sorting into increasing order of chain length (since translo-

cation time increases with chain length), the nanopore-channel device can produce increasing, decreasing, or non-monotonic sorting orders, depending on the channel dimensions. Furthermore, we showed that the separation power per nanopore can actually be greater in devices that sort into non-monotonic and decreasing orders.

Finally, it is interesting to contrast the dynamics of the nanopore-channel devices studied here and the slit-well devices studied extensively in the literature[3]. As pointed out above, the devices differ at a fundamental level because the slit-well device has one completely unconfined dimension, whereas the nanopore-channel device has none. Nonetheless, we recover the counter-intuitive result that longer polymers can traverse the nanopore-channel device more quickly than smaller polymers.

SUPPLEMENTARY MATERIAL

See supplementary material for additional details concerning the model and simulation implementations.

ACKNOWLEDGEMENTS

HWdH gratefully acknowledges funding from the Natural Sciences and Engineering Research Council (NSERC) in the form of Discovery Grant 2014-06091. MM gratefully acknowledges funding from the Ontario Graduate Scholarship (OGS).

[1]R. Mulero, A. S. Prabhu, K. J. Freedman, and M. J. Kim, JALA: Journal of the Association for Laboratory Automation **15**, 243 (2010).

[2]S. L. Levy and H. G. Craighead, Chemical Society Reviews **39**, 1133 (2010).

[3]K. D. Dorfman, Reviews of Modern Physics **82**, 2903 (2010).

[4]D. Branton, D. W. Deamer, A. Marziali, H. Bayley, S. A. Benner, T. Butler, M. Di Ventra, S. Garaj, A. Hibbs, X. Huang, S. B. Jovanovich, P. S. Krstic, S. Lindsay, X. S. Ling, C. H. Mastrangelo, A. Meller, J. S. Oliver, Y. V. Pershin, J. M. Ramsey, R. Riehn, G. V. Soni, V. Tabard-Cossa, M. Wanunu, M. Wiggin, and J. A. Schloss, Nature Biotechnology **26**, 1146 (2008).

[5]S. Carson, J. Wilson, A. Aksimentiev, and M. Wanunu, Biophysical Journal **107**, 2381 (2014).

[6]N. A. Bell, M. Muthukumar, and U. F. Keyser, Physical Review E **93**, 022401 (2016).

[7]K. Briggs, G. Madejski, M. Magill, K. Kastritis, H. W. de Haan, J. L. McGrath, and V. Tabard-Cossa, Nano Letters **18**, 660 (2018).

[8]J. C. Giddings, *Unified separation science* (Wiley, 1991).

[9]J.-L. Viovy, Reviews of Modern Physics **72**, 813 (2000).

[10]R. K. Harstad, A. C. Johnson, M. M. Weisenberger, and M. T. Bowser, Analytical Chemistry **88**, 299 (2015).

[11]J. Han and H. Craighead, Journal of Vacuum Science & Technology A: Vacuum, Surfaces, and Films **17**, 2142 (1999).

[12]J. Han and H. G. Craighead, Science **288**, 1026 (2000).

[13]M. Langecker, D. Pedone, F. C. Simmel, and U. Rant, Nano Letters **11**, 5002 (2011).

[14]G. W. Slater, C. Holm, M. V. Chubynsky, H. W. de Haan, A. Dubé, K. Grass, O. A. Hickey, C. Kingsburry, D. Sean, T. N. Shendruk, and L. Zhan, Electrophoresis **30**, 792 (2009).

[15]C. Forrey and M. Muthukumar, The Journal of Chemical Physics **127**, 015102 (2007).

[16]T. Ikonen, A. Bhattacharya, T. Ala-Nissila, and W. Sung, Physical Review E **85**, 051803 (2012).

[17]J. L. A. Dubbeldam, V. G. Rostiashvili, A. Milchev, and T. A. Vilgis, Physical Review E **85**, 041801 (2012).

[18]V. V. Lehtola, R. P. Linna, and K. Kaski, Physical Review E **78**, 061803 (2008).

[19]V. V. Lehtola, R. P. Linna, and K. Kaski, EPL (Europhysics Letters) **85**, 58006 (2009).

[20]V. V. Lehtola, K. Kaski, and R. P. Linna, Physical Review E **82**, 031908 (2010).

[21]V. V. Lehtola, R. P. Linna, and K. Kaski, Physical Review E **81**, 031803 (2010).

[22]R. P. Linna and K. Kaski, Physical Review E **85**, 041910 (2012).

[23]K. Luo, T. Ala-Nissila, S.-C. Ying, and R. Metzler, EPL (Europhysics Letters) **88**, 68006 (2009).

[24]J. L. A. Dubbeldam, V. G. Rostiashvili, A. Milchev, and T. A. Vilgis, Physical Review E **87**, 032147 (2013).

[25]A. Bhattacharya, W. Morrison, K. Luo, T. Ala-Nissila, S.-C. Ying, A. Milchev, and K. Binder, The European Physical Journal E **29**, 423 (2009).

[26]S. C. Vollmer and H. W. de Haan, The Journal of Chemical Physics **145**, 154902 (2016).

[27]H.-J. Limbach, A. Arnold, B. A. Mann, and C. Holm, Computer Physics Communications **174**, 704 (2006).

[28]D. Stigter, Biopolymers **16**, 1435 (1977).

[29]E. Sobel and J. Harpst, Biopolymers **31**, 1559 (1991).

[30]A. Savelyev, Physical Chemistry Chemical Physics **14**, 2250 (2012).

[31]A. R. Klotz, L. Duong, M. Mamaev, H. W. de Haan, J. Z. Chen, and W. W. Reisner, Macromolecules **48**, 5028 (2015).

[32]F. Farahpour, A. Maleknejad, F. Varnik, and M. R. Ejtehadi, Soft Matter **9**, 2750 (2013).

[33]H. W. de Haan, D. Sean, and G. W. Slater, Physical Review E **91**, 022601 (2015).

[34]M. Alnæs, J. Blechta, J. Hake, A. Johansson, B. Kehlet, A. Logg, C. Richardson, J. Ring, M. E. Rognes, and G. N. Wells, Archive

of Numerical Software **3**, 9 (2015).

[35] J. Mendeka, *Polymer Solutions* (Wiley Online Library, 2002).

[36] W. R. Inc., "Mathematica, Version 11.1," Champaign, IL, 2017.

[37] S. Redner, *A guide to first-passage processes* (Cambridge University Press, 2001).

[38] M. Magill, C. Falconer, E. Waller, and H. W. de Haan, Physical Review Letters **117**, 247802 (2016).

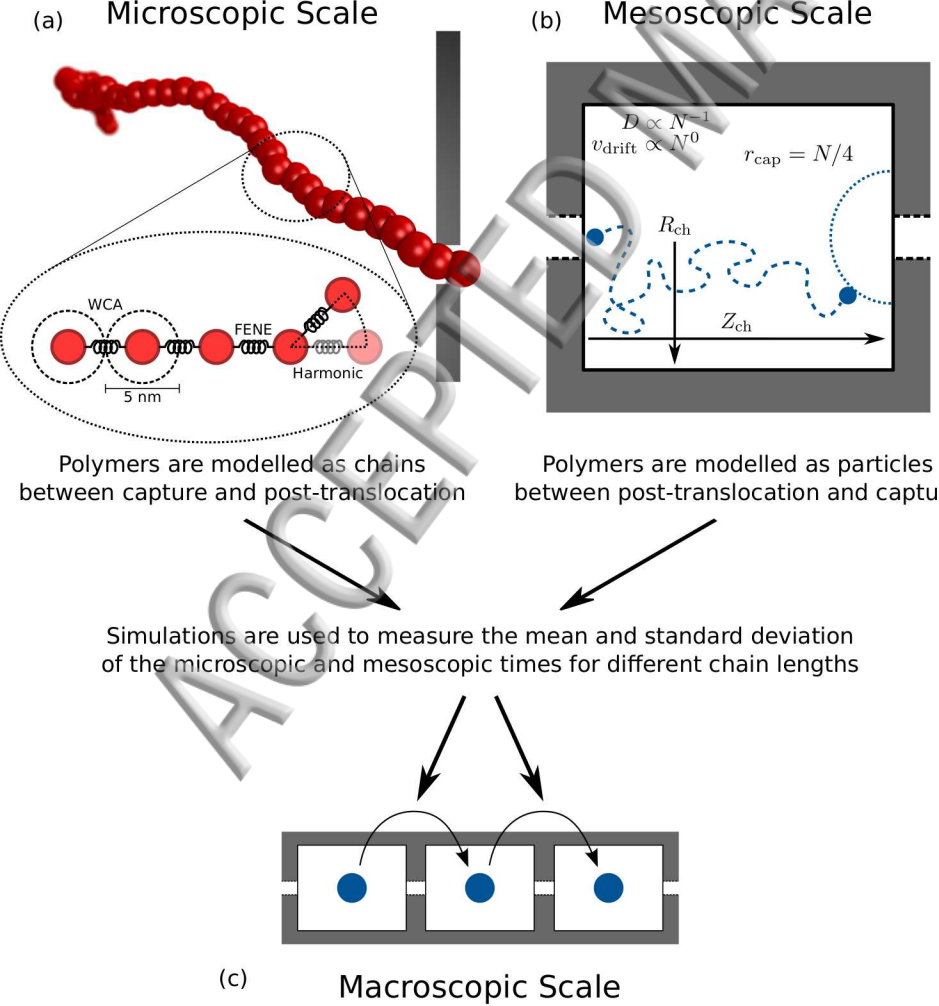

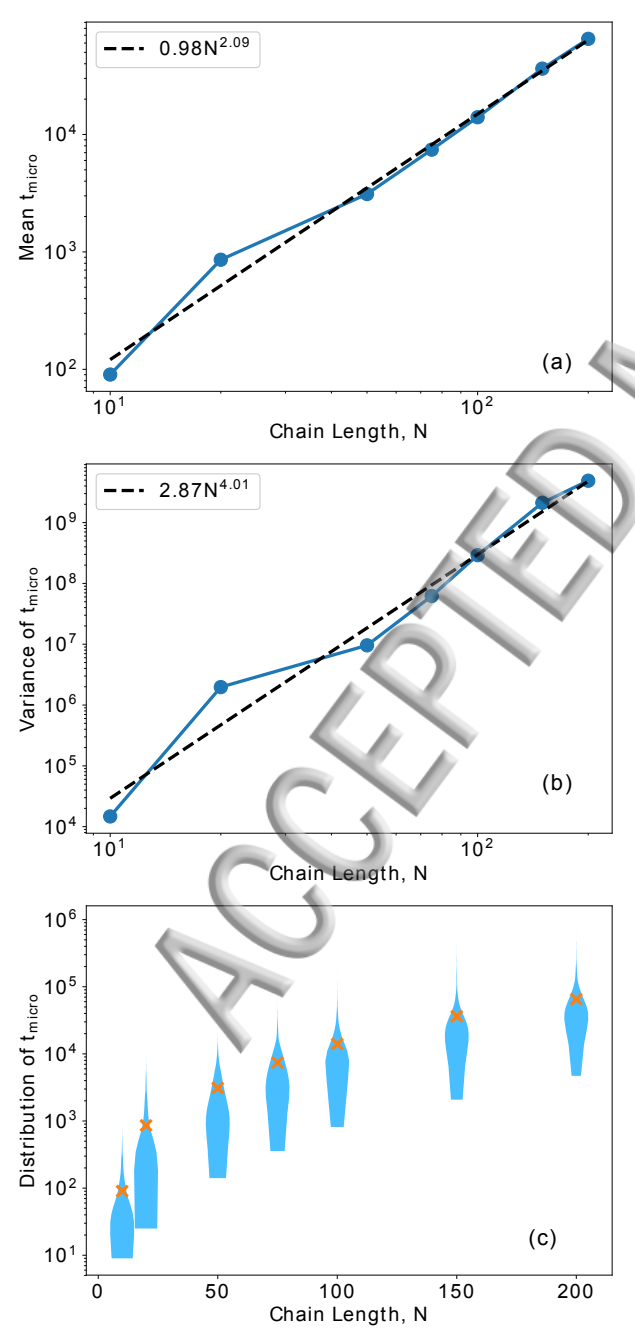
0.98N^2.09
Mean t_micro
Chain Length, N
(a)
2.87N^4.01
Variance of t_micro
Chain Length, N
(b)
Distribution of t_micro
Chain Length, N
(c)

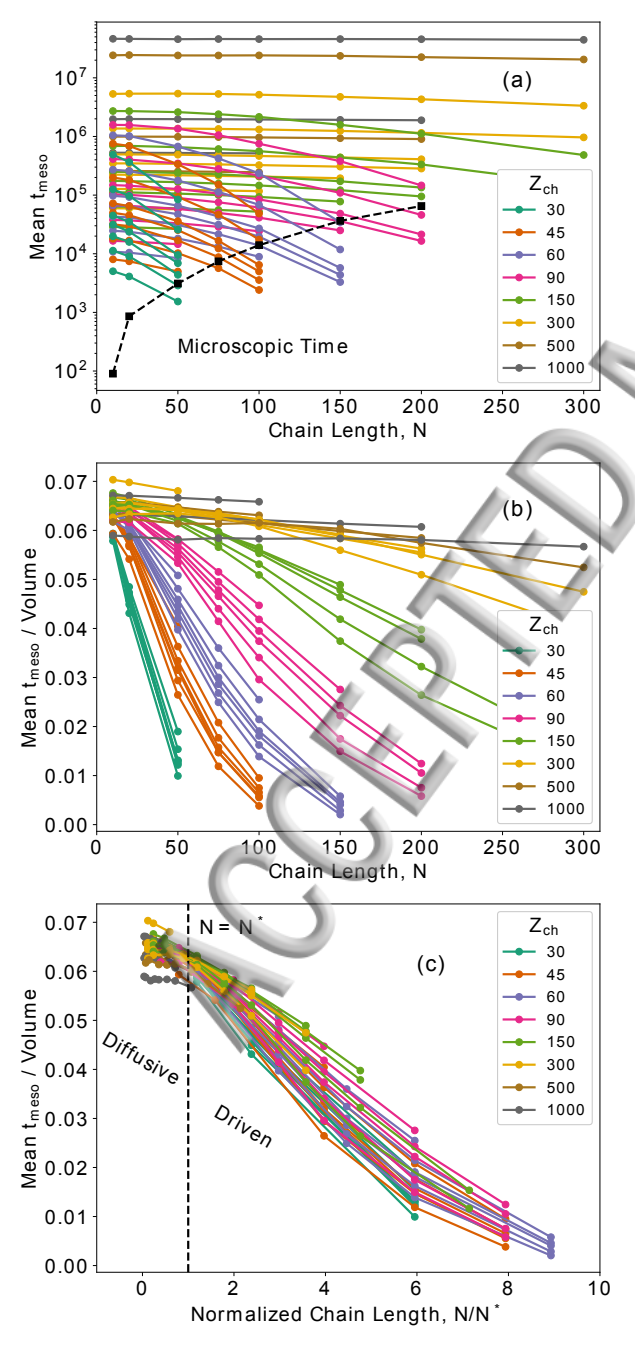
(a)
Mean t_{meso}
Microscopic Time
Chain Length, N
Z_{ch}
30
45
60
90
150
300
500
1000
(b)
Mean t_{meso} / Volume
Chain Length, N
(c)
N = N*
Diffusive
Driven
Normalized Chain Length, N/N*

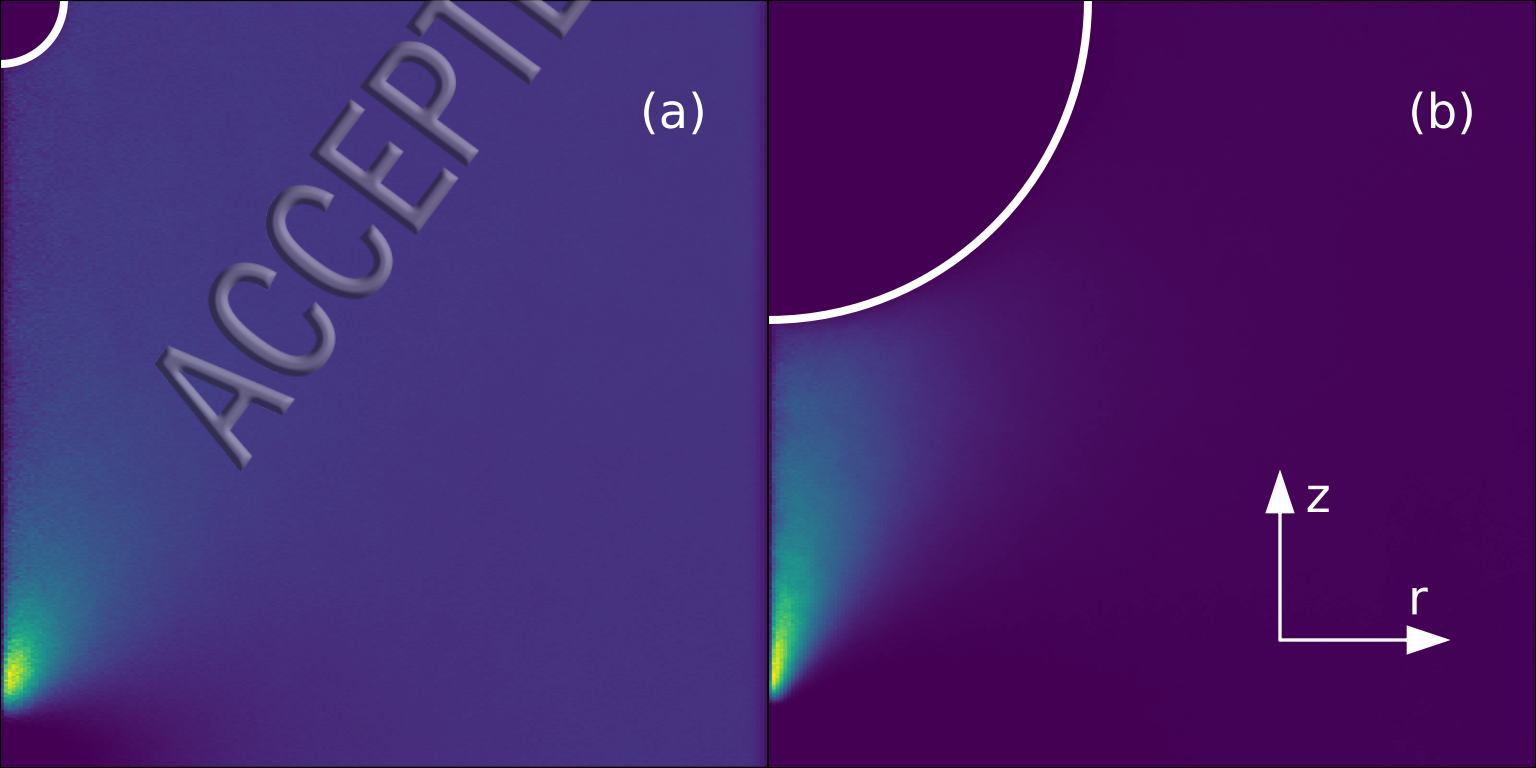
(a)
(b)
z
r

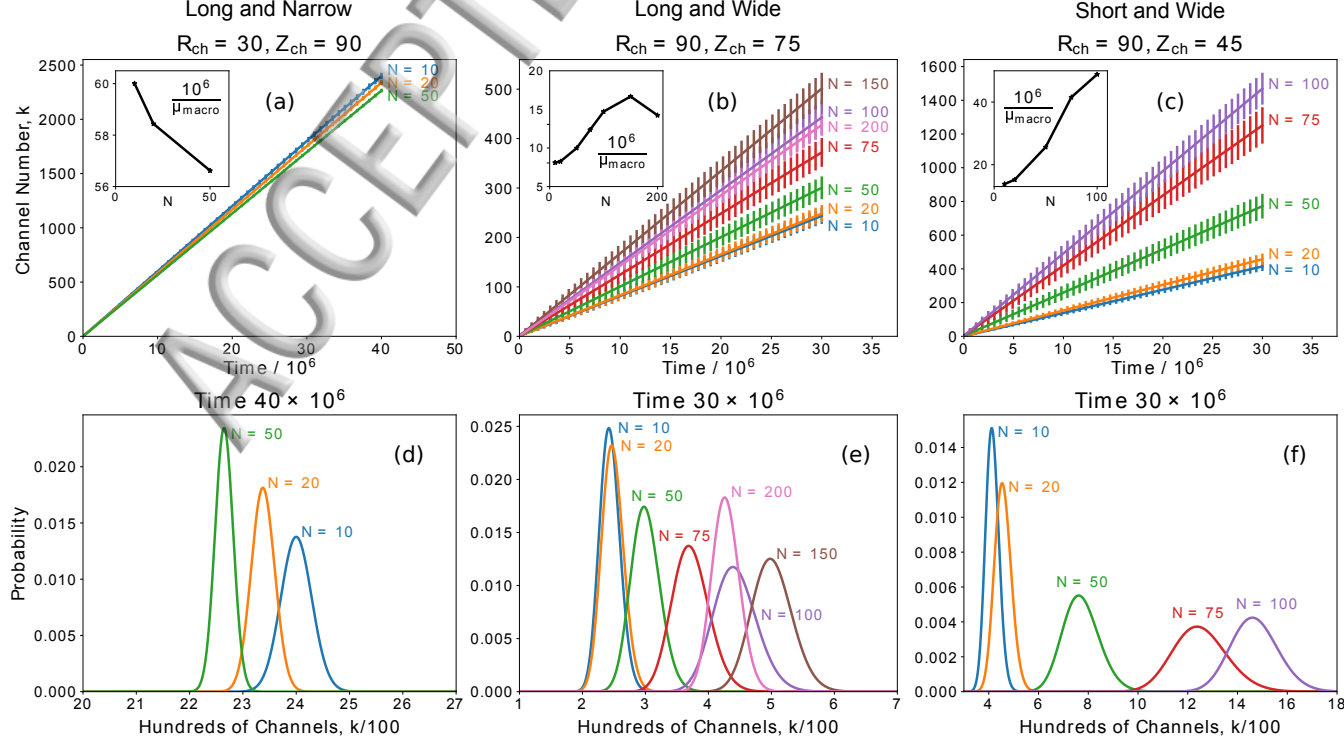
Long and Narrow
Rch = 30, Zch = 90
(a)
Channel Number, k
Time / 10^6
N = 10
N = 20
N = 50
10^6 / μmacro
N
Long and Wide
Rch = 90, Zch = 75
(b)
N = 150
N = 100
N = 200
N = 75
N = 50
N = 20
N = 10
Short and Wide
Rch = 90, Zch = 45
(c)
N = 100
N = 75
N = 50
N = 20
N = 10
Time 40 × 10^6
(d)
Probability
Hundreds of Channels, k/100
Time 30 × 10^6
(e)
(f)